Effect of poloidal asymmetries on impurity peaking in tokamaks

A. Mollén, I. Pusztai, T. Fülöp, Ye. O. Kazakov, and S. Moradi
Department of Applied Physics, Nuclear Engineering, Chalmers University of Technology and Euratom-VR Association, Göteborg, Sweden

(Received 25 January 2012; accepted 22 April 2012; published online 30 May 2012)

Poloidal impurity asymmetries are frequently observed in tokamaks. In this paper, the effect of poloidal asymmetry on electrostatic turbulent transport is studied, including the effect of the $\mathbf{E} \times \mathbf{B}$ drift. Collisions are modeled by a Lorentz operator, and the gyrokinetic equation is solved with a variational approach. The impurity transport is shown to be sensitive to the magnetic shear and changes sign for $s \gtrsim 0.5$ in the presence of inboard accumulation. The zero-flux impurity density gradient (peaking factor) is shown to be rather insensitive to collisions in both ion temperature gradient and trapped electron mode driven cases. Our results suggest that the asymmetry (both the location of its maximum and its strength) and the magnetic shear are the two most important parameters that affect the impurity peaking. [http://dx.doi.org/10.1063/1.4719711]

I. INTRODUCTION

The accumulation of impurities in the core of a fusion plasma has debilitating effect on fusion reactivity due to an increase in radiation losses and plasma dilution. Significant effort has been spent finding conditions in which accumulation in the plasma core can be avoided. This includes the characterization of cross-field impurity transport, which in recent years has moved towards finding ways to actively control the concentration of impurities in the core. One of the ways to influence the impurity transport is to provide additional central heating which has been shown to give a flattening effect on the density profiles of impurities in the core,[1–5] for reasons that are still not properly understood. Recent work noted that the impurity cross-field transport driven by electrostatic turbulence depends on the poloidal asymmetry of the impurities,[6,7] and this, along with other effects, may be a contributing factor to the avoidance of accumulation of impurities with high charge numbers.

Poloidally asymmetric impurity distributions in tokamaks were studied already in the 1970s (Ref. 8), and their effect on neoclassical impurity transport has been discussed before.[9–12] Today there is a wealth of experimental evidence for poloidal asymmetries, for an overview of impurity asymmetry measurements organized by experiment see Ref. 13. Asymmetries can arise due to various reasons, e.g., difference in impurity source location, toroidal plasma rotation, neoclassical effects, or radio frequency (RF) heating. In this paper, the emphasis will be on the effect of RF heating in the plasma core and in particular the study of inboard accumulation.

One of the first accounts of ion cyclotron resonance heating (ICRH) driven inboard accumulation of impurities was given in Ref. 14, where asymmetry in the soft x-ray emission was observed during the injection of nickel. Also in the Alcator C-Mod tokamak strong poloidal asymmetries in molybdenum density are observed in plasmas using ICRH.[15] The RF heating scheme applied in both cases is hydrogen minority heating in a deuterium plasma. The heating gives rise to a poloidal asymmetry in the density of minority ions, and this induces an electric field which pushes the impurities to the inboard side. Although the poloidal electric field induced by RF is too small to lead to poloidal asymmetries in the background electron and ion densities, it may influence the dynamics of impurities with high charge numbers.

The purpose of this paper is to study the effect of the $\mathbf{E} \times \mathbf{B}$ drift of the impurities in the presence of poloidal asymmetry and thereby extend previous work on impurity transport driven by electrostatic turbulence.[7] We will show that a poloidally varying electrostatic potential—arising due to, e.g., RF heating, parallel friction due to large gradients, or other effects—can lead to a strong reduction or sign change of the zero-flux impurity density gradient (impurity peaking factor). The poloidal variation of the potential has two fold effect; magnified by the charge of the impurities, it can lead to a significant impurity asymmetry which, provided being sufficiently strong, can lead to a sign change in the impurity peaking factor in itself as it was shown in Ref. 7. But more important, the sign change of the impurity peaking factor can happen at much weaker asymmetry strengths than was considered in Ref. 7, aided by the $\mathbf{E} \times \mathbf{B}$ drift of impurities in the poloidally varying equilibrium potential. The peaking factor of highly charged impurities depends mainly on magnetic shear and the form of the poloidally varying equilibrium potential (both the location of its maximum and its strength). It will be shown that the reduction of the peaking factor is specially pronounced in regions of moderate shear $s \gtrsim 0.5$, where even a sign change can occur for inboard accumulation. Furthermore, in this paper, we model impurity-impurity collisions by employing a Lorentz operator and solve the gyrokinetic (GK) equation with a variational method. Our study concludes, however, that impurity-impurity collisions will not affect the cross-field transport of impurities significantly.

The rest of the paper will be organized as follows: In Sec. II, we formulate the model for calculating the impurity flux and the peaking factor, including the $\mathbf{E} \times \mathbf{B}$ drift and collisions (details of the derivation will be given in the Appendices). In Sec. III, we describe the ICRH induced asymmetry. Here, a model for the RF heated minority ions is linked to the asymmetry of impurity ions, and reasonable

asymmetry strengths that could be caused by ICRH are estimated. Furthermore, we derive an approximate expression for the peaking factor in the high charge number limit. Section IV contains the parametric dependences of the peaking factor on charge number, asymmetry, shear, density and temperature gradients and collisions. Finally, the results are summarized in Sec. V.

II. IMPURITY FLUX

Impurity cross-field transport is usually dominated by drift-wave turbulence; consequently, this work is focused on the effect of poloidally asymmetric impurity distributions on impurity transport driven by microinstabilities. It is assumed that the fluctuations responsible for the cross-field transport do not significantly affect the processes causing the poloidal asymmetry. The quasilinear impurity flux driven by electrostatic microinstabilities is given by

$$\Gamma_z = -\frac{k_\theta}{B}\Im[\hat{n}_z\phi^*] = -\frac{k_\theta}{B}\Im\left[\int d^3v J_0(z_z) g_z \phi^*\right], \quad (1)$$

where $\Im[\cdot]$ denotes the imaginary part, k_θ is the poloidal wave-number, $\hat{n}_z$ is the perturbed impurity density, g_z is the non-adiabatic part of the perturbed impurity distribution function, J_0 is the Bessel function of the first kind, $z_z = k_\perp v_\perp/\omega_{cz}, \omega_{cz} = ZeB/m_z$ is the cyclotron frequency, and $k_\perp = (1+s^2\theta^2)^{1/2}k_\theta$. Furthermore, m_z and Z are the impurity mass and charge number, respectively, ϕ^* is the complex conjugate of the perturbed electrostatic potential, and B is the strength of the equilibrium magnetic field. The subscripts $\parallel$ and $\perp$ denote the parallel and perpendicular directions with respect to the magnetic field.

In this work, we will order the equilibrium electrostatic potential so that $e\phi_E/T_j \ll 1$, where T_j is the temperature of species j. Thus, the main ion and electron distributions are poloidally symmetric, but we allow for high enough charge numbers of the impurities so that $Ze\phi_E/T_z = \mathcal{O}(1)$. For simplicity, we consider an axisymmetric, large aspect-ratio torus with circular magnetic surfaces. θ and r denote the poloidal and radial coordinates, respectively. The non-adiabatic part of the perturbed distribution function g_z can be obtained from the linearized GK equation

$$\frac{v_\parallel}{qR}\frac{\partial g_z}{\partial\vartheta} - i(\omega-\omega_{Dz}-\omega_E)g_z - C(g_z) = -i\frac{Zef_{z0}}{T_z}(\omega-\omega_{*z}^T)\phi J_0(z_z), \quad (2)$$

where ϑ is the extended poloidal angle, $\omega = \omega_r + i\gamma$ is the mode frequency, $f_{z0} = n_{z0}(m_z/2\pi T_z)^{3/2}\exp(-\mathcal{E}/T_z)$ is the equilibrium Maxwellian distribution function, $\mathcal{E} = m_z v^2/2 + Ze\phi_E$ is the total energy, $n_z(\mathbf{r}) = n_{z0}\exp[-Ze\phi_E(\mathbf{r})/T_z]$ is the poloidally varying impurity density, and n_{z0} is a flux function. The diamagnetic frequency is defined as $\omega_{*z} = -k_\theta T_z/ZeBL_{nz}$ and $\omega_{*z}^T = \omega_{*z}[1 - L_{nz}Ze\partial\phi_E/\partial r/T_z + (\mathcal{E}/T_z - Ze\phi_E/T_z - 3/2)L_{nz}/L_{Tz}]$, with $L_{nz} = -[\partial(\ln n_z)/\partial r]^{-1}$ and $L_{Tz} = -[\partial(\ln T_z)/\partial r]^{-1}$ being the density and temperature scale lengths, respectively, and $\mu = m_z v_\perp^2/(2B)$ is the magnetic moment. The magnetic drift frequency is $\omega_{Dz} = -2k_\theta(\mathcal{E} - Ze\phi_E - \mu B/2)\mathcal{D}(\vartheta)/(m_z\omega_{cz}R)$, where $\mathcal{D}(\vartheta) = \cos\vartheta + s\vartheta\sin\vartheta$, q is the safety factor and $s = (r/q)(dq/dr)$ is the magnetic shear. The quantity ω_E stems from the $\mathbf{E}\times\mathbf{B}$ drift of the particles in the equilibrium electrostatic field and has the form (see Appendix A)

$$\omega_E = \frac{k_\theta}{B}\left[\frac{\partial\phi_E}{\partial r} - \frac{s\vartheta}{r}\frac{\partial\phi_E}{\partial\vartheta}\right]. \quad (3)$$

Henceforth, rotation will be neglected and we put $\partial\phi_E/\partial r = 0$ in Eq. (3) and in ω_{*z}^T and write $E_\theta \times B_\varphi$ when we refer to the $\mathbf{E}\times\mathbf{B}$ drift in the poloidally varying electric field. Also in the following, the parallel dynamics and the trapping of impurities due to $\nabla_\parallel B$ and $\nabla_\parallel\phi_E$ are neglected and, for simplicity, also finite Larmor-radius (FLR) effects are omitted [$J_0(z_z) = 1$ is taken in Eqs. (1) and (2)]; these assumptions are justified for heavy impurities with low thermal velocity if $m_z \propto Z$. Accordingly, the equation we need to solve is

$$-i(\omega-\omega_{Dz}-\omega_E)g_z - C(g_z) = -i\frac{Zef_{z0}}{T_z}(\omega-\omega_{*z}^T)\phi. \quad (4)$$

If $n_z Z^2/n_e$ is of order unity or larger, the impurity-impurity collisions dominate over collisions between impurities and other species, even if the collision frequencies with the other species can be formally comparable to the impurity-impurity collision frequency. The reason for this can be seen from, e.g., Eq. (41) in chap. 5.2 of Ref. 16, where all factors in the collision time are the same for zi and zz collision times except $v_{t>}$ in the numerator. Here, $v_{t>}$ is the largest of the two thermal speeds. This leads to $\tau_{zz}/\tau_{zi} = v_{tz}/v_{ti} \ll 1$ if $Z \gg 1$. Therefore, it is sufficient to consider only the impurity self-collisions which can be modeled by a pitch angle scattering operator and a term to restore momentum conservation. Since the motion of impurities is slow compared to other species, momentum conservation is not expected to affect the results on turbulence time scales. Thus, we model impurity collisions with the Lorentz operator

$$C(g_z) = \frac{\nu_D(x)}{2}\mathcal{L}(g_z) \equiv \frac{\nu_D(x)}{2}\frac{\partial}{\partial\xi}\left[(1-\xi^2)\frac{\partial g_z}{\partial\xi}\right], \quad (5)$$

where ν_D is the deflection frequency for self-collisions $\nu_D(x) = \hat{\nu}_{zz}[\mathrm{Erf}(x) - G(x)]/x^3$, $x = v/v_{Tz}$ represents velocity normalized to the thermal speed $v_{Tz} = (2T_z/m_z)^{1/2}$, $\hat{\nu}_{zz} = n_z Z^4 e^4 \ln\Lambda/\ [4\pi\epsilon_0^2 m_z^{1/2}(2T_z)^{3/2}]$, and $\ln\Lambda$ is the Coulomb logarithm. $\mathrm{Erf}(x)$ is the error-function, and $G(x) = [\mathrm{Erf}(x) - x\mathrm{Erf}'(x)]/(2x^2)$ the Chandrasekhar function. In the Lorentz operator, $\xi = x_\parallel/x$ denotes the cosine of the pitch-angle.

The Lorentz operator makes the distribution more isotropic in velocity space in a diffusive way. The only anisotropy in Eq. (4) is in the magnetic drift term since it is proportional to $\mathcal{E} - Ze\phi_E - \mu B/2 = T_z(x_\parallel^2 + x_\perp^2/2)$. In the constant energy resonance (CER) approximation $[v_\perp^2 + 2v_\parallel^2 \to 4(v_\perp^2 + v_\parallel^2)/3]$, Eq. (4) would be isotropic and pitch-angle scattering would have no effect at all. It should

be noted, however, that in the full linear GK equation (2), both the parallel compressibility and the Bessel function representing FLR-effects introduce some anisotropy; however, these terms can be neglected for heavy impurities as mentioned above. The anisotropy from the magnetic drifts can be written in terms of Legendre polynomials $P_l(\xi)$, that are the eigenfunctions of the operator $\mathcal{L}$, as $\omega_{Dz} = [2P_0(\xi) + P_2(\xi)]\omega_{Dx}/3$, where $\omega_{Dx} = -k_\theta v_{Tz}^2 x^2(\cos\vartheta + s\vartheta\sin\vartheta)/(\omega_{cz}R)$. Using this form, an approximate variational solution of the GK equation including collisions modeled by a Lorentz operator can be derived as a truncated Legendre polynomial series; the details of this calculation are given in Appendix B. In Sec. II A, we use the variational solution given in Eq. (5) to calculate the peaking factor.

A. Zero-flux impurity density gradient

Using the formula for the quasilinear particle flux for impurities, Eq. (1), the normalized zero-flux impurity density gradient a/L_{nz}^0 can be obtained from the requirement that the flux surface average of the particle flux vanishes $\langle\Gamma_z\rangle = 0$, where $\langle\cdot\rangle = (1/2\pi)\int_{-\pi}^{\pi}(\cdot)\,d\theta$. Here, a is the outermost minor radius. We neglect the contribution from the part of the potential that is outside the extended angle interval $[-\pi,\pi]$, which means that our expression is not valid in cases where the ballooning eigenfunction is very elongated. We perform the integration over velocity space using the energy and magnetic moment normalized to temperature, $\tilde{\mathcal{E}} = \mathcal{E}/T_z$ and $\tilde{\mu} = \mu/T_z$, as velocity space coordinates. Accordingly, we have

$$\int d^3v = \pi v_{Tz}^3 \int_{Ze\phi_E/T_z}^{\infty} d\tilde{\mathcal{E}} \int_0^{(\tilde{\mathcal{E}}-Ze\phi_E/T_z)/B} d\tilde{\mu}\frac{B}{\sqrt{\tilde{\mathcal{E}}-\tilde{\mu}B-Ze\phi_E/T_z}},$$

and the peaking factor can be written as

$$\frac{a}{L_{nz}^0} = \frac{\mathcal{P}_T}{\mathcal{P}_n}, \tag{6}$$

where

$$\mathcal{P}_T = \left\langle \Re\left[\int d\tilde{\mathcal{E}}\int d\tilde{\mu}\frac{\exp(-\tilde{\mathcal{E}})|\phi|^2A(x)}{\sqrt{\tilde{\mathcal{E}}-\tilde{\mu}B-Ze\phi_E/T_z}} \times\left\{\bar{\omega}-\bar{\omega}_{*z}\left(\tilde{\mathcal{E}}-\frac{Ze\phi_E}{T_z}-\frac{3}{2}\right)\frac{a}{L_{Tz}}\right\}\right]\right\rangle,$$

$$\mathcal{P}_n = \left\langle \Re\left[\int d\tilde{\mathcal{E}}\int d\tilde{\mu}\frac{\exp(-\tilde{\mathcal{E}})|\phi|^2A(x)}{\sqrt{\tilde{\mathcal{E}}-\tilde{\mu}B-Ze\phi_E/T_z}}\bar{\omega}_{*z}\right]\right\rangle,$$

and $\Re[\cdot]$ denotes real part. In the integrals above, $\tilde{\mathcal{E}}$ is integrated over $[Ze\phi_E/T_z,\infty]$ and $\tilde{\mu}$ over $[0,(\tilde{\mathcal{E}}-Ze\phi_E/T_z)/B]$. Furthermore, we introduced

$$A(x) = \frac{5[7\bar{F}_0(x)+2\bar{F}_2(x)+21\bar{\nu}_D(x)]}{35\bar{F}_0^2(x)+10\bar{F}_0(x)\bar{F}_2(x)-7\bar{F}_2^2(x)+105\bar{F}_0(x)\bar{\nu}_D(x)}, \tag{7}$$

where $\bar{F}_0(x) = -i(\bar{\omega}-2\bar{\omega}_{D0}x^2/3-\bar{\omega}_E)$, $\bar{F}_2(x) = i\bar{\omega}_{D0}x^2/3$. The bar signifies that the parameter is given in c_s/a units, where $c_s = (T_e/m_i)^{1/2}$ is the ion sound speed. $\bar{\omega} = a\omega/c_s$ is the normalized wave frequency, $\bar{\omega}_{*z} = -k_\theta\rho_{s0}(1+\epsilon\cos\vartheta)/(Z\tau_z)$ is the normalized diamagnetic frequency, $\bar{\omega}_{D0} = -2k_\theta\rho_{s0}a(\cos\vartheta + s\vartheta\sin\vartheta)/(R_0Z\tau_z)$ is the normalized drift frequency, and

$$\bar{\omega}_E = -\frac{a}{r}s\vartheta\frac{Ze}{T_z}\frac{\partial\phi_E}{\partial\vartheta}\frac{k_\theta\rho_{s0}}{Z\tau_z}(1+\epsilon\cos\vartheta)$$

is the normalized $E_\theta\times B_\varphi$ drift frequency, with $\tau_z = T_e/T_z$. ρ_{s0} denotes the ion sound Larmor radius $\rho_s = c_s/\omega_{ci}$ at R_0 and $\epsilon = r_0/R_0$ is the inverse aspect ratio, where r_0 is the local reference minor radius and R_0 is the major radius of the magnetic axis. The equation for the velocity dependent $A(x)$ factor (7) comes from $A_1(x,\xi)/A_2(x)$ appearing in Eq. (B5) in Appendix B, after dropping the $P_2(\xi)$ term in A_1 that vanishes upon velocity integration.

The normalized deflection frequency is $\bar{\nu}_D(x) = (n_z/n_i)Z^4\tau_z^2\bar{\nu}_{ei}(m_e/m_z)^{1/2}\,[\mathrm{Erf}(x)-G(x)]/x^3$. Expressed in $\tilde{\mathcal{E}}$ and $\tilde{\mu}$ variables, the normalized speed is $x = (\tilde{\mathcal{E}}-Ze\phi_E/T_z)^{1/2}$, and the cosine of the pitch angle is $\xi = [1-\tilde{\mu}B/(\tilde{\mathcal{E}}-Ze\phi_E/T_z)]^{1/2}$.

III. MODEL FOR THE POLOIDAL ASYMMETRY

We assume that the plasma consists of electrons (e), deuterium ions (i), impurity ions (z), and RF heated hydrogen minority ions (H). The equilibrium distribution of each particle species (α) except the minority ions can be expected to be a Boltzmann distribution (the dynamics of the minority ions is strongly affected by the RF heating): $n_\alpha = n_{\alpha0}\exp(-e_\alpha\phi_E/T_\alpha) \approx n_{\alpha0}(1-e_\alpha\phi_E/T_\alpha)$, where e_α is the charge, T_α is the temperature of the species (approximately constant on a flux surface), and ϕ_E is the equilibrium potential. The subscript zero indicates the density where the equilibrium potential vanishes. Here, in order to get a simple approximate expression for the poloidally varying potential, we assume that the linear expansion in $Ze\phi_E/T_z$ of the Boltzmann distributed impurities is valid (while in other parts of the paper we allow this parameter to be order unity); this is a reasonable approximation for experimentally relevant values of $Ze\phi_E/T_z$. This implies that the poloidal variation of the density on a flux surface $\tilde{n}_\alpha = n_\alpha - n_{\alpha0}$ is given by $\tilde{n}_\alpha/n_{\alpha0} \simeq -e_\alpha\phi_E/T_\alpha$. Assuming that the poloidal variation in the potential ϕ_E is produced by the poloidally asymmetric distribution of the heated minority ions, from quasineutrality, we can derive an expression for the impurity density on a flux surface

$$\frac{n_z}{n_{z0}} = \exp\left(-\frac{Ze\phi_E}{T_z}\right) = \exp\left(-\frac{Z\hat{n}_H/n_{e0}}{(T_z/T_i)(n_{i0}/n_{e0})+(T_z/T_e)+(n_{z0}Z^2/n_{e0})}\right), \tag{8}$$

where $\hat{n}_H$ represents the fraction of the hydrogen minority density which feels the ICRH resonance and does not follow a Boltzmann distribution. Here, ϕ_E is normalized so that

$n_{i0} + n_{H0} + Zn_{z0} - n_{e0} = 0$. The poloidal variation enters through $\hat{n}_H = \hat{n}_H(\theta)$. Since the exponent in Eq. (8) is negative, a maximum in $\hat{n}_H$ corresponds to a minimum in n_z; hence, accumulation of minority ions on the outboard side gives rise to an electric field that pushes the impurities to the inboard side.

The minority density becomes poloidally asymmetric if ICRH is applied. Equation (8) shows that one of the most important factors affecting the poloidally asymmetric impurity accumulation is the fraction of the minority density. We can obtain a simple estimate for this by using the *ansatz* for the distribution function of minority ions heated by ICRH given in Ref. 17,

$$f_H(\mathcal{E},\mu) = \left(\frac{m_H}{2\pi}\right)^{3/2} \frac{n_c(r)}{T_\perp(r)T_{||}^{1/2}(r)} \exp\left[-\frac{\mu B_c}{T_\perp(r)} - \frac{|\mathcal{E}-\mu B_c|}{T_{||}(r)}\right]. \tag{9}$$

Here, m_H is the mass of the hydrogen minority ions, B_c is the ICRH resonant magnetic field strength, and n_c is the minority density along the ICRH resonance layer. Since ICRH causes minority ion acceleration dominantly across the magnetic field, the effective minority perpendicular temperature at the resonance region is usually much higher than the parallel one. From Eq. (9), it can be shown that if the resonance layer is at the low field side and does not intersect the studied flux surface, the poloidal variation of the potential is expected to be sinusoidal to first order. The asymmetry strength depends on $b_c = B_c/B_0$ (here, B_0 is the magnetic field at the magnetic axis), minority temperature anisotropy $\alpha_T = T_\perp/T_{||}$, and minority concentration n_{H0}/n_e (Ref. 18), as

$$n_H(\theta) \approx n_{H0}(1 + k\cos\theta), k = \frac{\epsilon\, b_c(\alpha_T - 1)}{b_c + \alpha_T(1 - b_c)}. \tag{10}$$

Being related to the hydrogen minority concentration, the poloidal variation of the potential causes impurities to be asymmetrically distributed over the flux surface. As follows from Eq. (10), this asymmetry is strengthened by high minority temperature anisotropy. We note that if the resonance layer intersects the studied flux surface then the poloidal distribution of the minorities cannot be well modeled with a simple sinusoidal approximation. Also when the resonance layer is at the high magnetic field side of the flux surface, this simple model is not accurate, and in these cases, Eq. (10) is not valid.

The electrostatic potential depends on various competing effects and is in general difficult to determine (or measure). Since in the present work we concentrate on the effects of the poloidal variation of ϕ_E, as earlier mentioned we ignore its radial variation, that is, we neglect toroidal rotation. We also assume that its poloidal dependence is approximately sinusoidal (as shown above in the case of ICRH driven asymmetries). This motivates the following *ansatz* for the equilibrium potential

$$Ze\phi_E/T_z = -\kappa\cos(\theta - \delta), \tag{11}$$

where δ represents the angular position where the impurity density has its maximum and κ sets the strength of the poloidal asymmetry. Thus, the impurity density will be assumed to vary according to $n_z(\theta, r) = n_{z0}(r)\exp[\kappa\cos(\theta - \delta)]$. In the model for ICRH driven asymmetries presented above, $\delta = \pi$ is obtained. Although electron cyclotron resonance heating (ECRH) is not quantitatively described by this model, we might expect that it will result in an outboard accumulation of impurities, corresponding to $\delta = 0$ (this possibility is mentioned in Ref. 13, although we are not aware of a detailed theoretical study on the topic). Accordingly, we will in our analysis present results with both $\delta = 0$ and $\delta = \pi$.

By comparing Eqs. (8) and (11) in the limit $n_{z0}Z^2/n_{e0} \ll 1$, it can be noted that the asymmetry strength is proportional to the impurity charge and the minority concentration, $\kappa \propto Z\hat{n}_H$. Figure 1(a) shows the asymmetry strength calculated from

$$\kappa = \frac{Z(n_{H0}/n_{e0})k}{(T_z/T_i)(n_{i0}/n_{e0}) + (T_z/T_e) + (n_{z0}Z^2/n_{e0})} \tag{12}$$

as a function of the minority temperature anisotropy α_T for various impurity species. Here, we assumed $n_{H0} \ll n_{i0}$. The asymmetry strength increases with impurity charge and minority temperature anisotropy. For ICRH powers of the order of 3 MW temperature anisotropies up to about $\alpha_T = 8$ can be expected.[17] Higher ICRH power leads to higher temperature anisotropies, but also other parameters matter (such as antenna phasing, background densities and temperatures, radius, etc). Equation (12) suggests that the asymmetry strength is proportional to the minority fraction, but it should be noted that the minority fraction affects the minority temperature anisotropy as well. Too high minority fraction will change the mode of heating (from ion to electron heating). The anisotropy of the distribution function is reduced with minority concentration, since the deposited energy per particle is reduced. To get the same level of anisotropy with higher minority concentration, higher ICRH power is needed. Note that in case of small impurity fraction (so that Z^2n_{z0}/n_{e0} can be dropped in the denominator of Eq. (12)), the asymmetry strength κ is larger. Figure 1(b) shows how the impurity density varies with poloidal angle for different values of the strength.

In the following, we will refer to "in-out" and "out-in" asymmetries as the situations when the maximum of the poloidally varying impurity density is located at the high-field and low-field sides of the plasma, respectively.

Note that the poloidal distribution of impurities corresponding to the potential given in Eq. (11) is different from the *ansatz* used in Ref. 7. The choice of Eq. (11) is convenient because this way the modeling of weak asymmetries ($\kappa < 1$) is more straightforward. In Refs. 6 and 7, the poloidal asymmetry of the impurity density was modeled by the *ansatz* $n_z = n_{z0}\mathcal{P}(\theta) = n_{z0}\sum_n f_n P(\theta,\delta,n)$, where $P(\theta,\delta,n) = \left[\cos^2\left(\frac{\theta-\delta}{2}\right)\right]^n$, with n representing the peakedness of the asymmetry (note that the asymmetry strength κ used in this paper is not equivalent with n) and the weights f_n could be chosen to represent populations of impurities with various degrees of peakedness. The *ansatz* used here with $\kappa = 0.5$

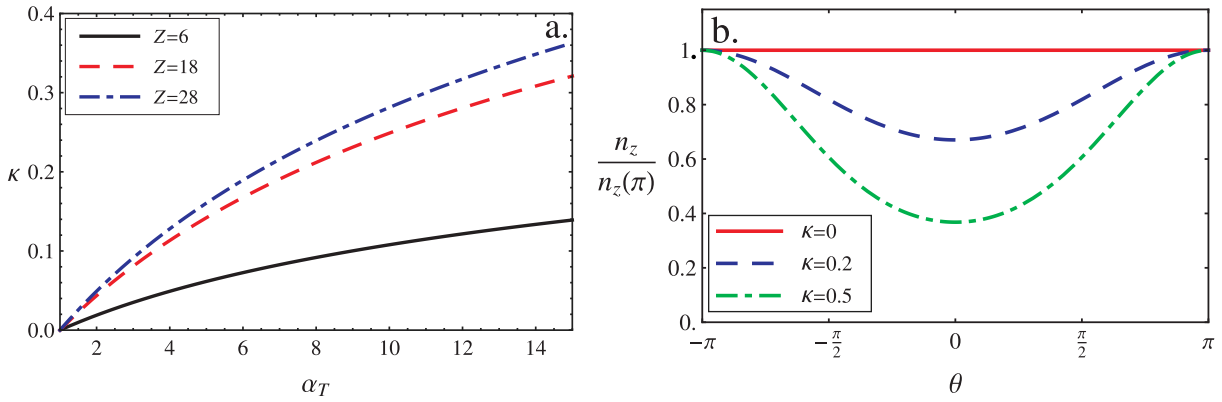

FIG. 1. (a) Asymmetry strength κ as a function of minority temperature anisotropy α_T for carbon ($Z=6$), argon ($Z=18$), and nickel ($Z=28$) with $n_{H0}/n_{e0}=0.07, n_{z0}/n_{e0}=2\times10^{-3}, b_c=0.91, T_i=T_z=0.85\,T_e$, and $\epsilon=0.1$. (b) Normalized poloidal impurity density variation for $\kappa=0, \kappa=0.2$ and $\kappa=0.5$ with $\delta=\pi$.

would correspond to $f_0=1$, $f_1=2$, and $\kappa=0.2$ corresponds to $f_0=1$, $f_1=0.5$ (the rest of f_j is equal to zero). In Ref. 7, mostly $n=3$ ($f_3=1, f_{j\neq3}=0$) was used to demonstrate the effect of the poloidally asymmetric impurity distribution, since rather strong asymmetry strength was necessary to get a sign change of the peaking factor without including the $E_\theta\times B_\varphi$ drift.

A. Approximate analytical solution for the peaking factor

If collisions are neglected one can construct an approximate analytical solution for the peaking factor by solving the integral in the expression for the perturbed impurity density analytically. This can be done if we employ the CER approximation in the expression for the magnetic drift so that we have

$$\hat{n}_z=\frac{Ze\phi n_z}{T_z}\left(-1+\int 4\pi x_z^2 dx_z\frac{e^{-x_z^2}}{\pi^{3/2}}\frac{\omega-\omega_{*z}^T}{\omega-\omega_E-x_z^2\hat{\omega}_{Dz}}\right),$$

where $\hat{\omega}_{Dz}=\omega_{Dz0}\mathcal{D}(\vartheta)$, with $\omega_{Dz0}=-2k_\theta v_{Tz}^2/3\omega_{cz}R$. To simplify the velocity integral, we can expand the integrand in the smallness of $1/Z$, noting that $\hat{\omega}_{Dz}, \omega_{*z}^T\propto 1/Z$, to obtain

$$\hat{n}_z=\frac{Ze\phi n_z}{T_z}\frac{1}{\omega-\omega_E}\left[\omega_E-\omega_{*z}+\frac{3\hat{\omega}_{Dz}}{2}+\frac{3\omega_E\hat{\omega}_{Dz}}{2(\omega-\omega_E)}\right]. \tag{13}$$

In general, the last two terms in the bracket in Eq. (13) can be of the same order of magnitude, since ω_E can be as large as $|\omega|$ and written in the form of Eq. (3), ω_E is seemingly independent of Z. However, when the $n_{z0}Z^2/n_{e0}$ term in the denominator in Eq. (8) is not negligibly small, $Ze\phi_E/T_z$ can be roughly constant for different values of Z. Keeping formally $Ze\phi_E/T_z$ constant leads to $\omega_E\sim 1/Z$. This means that the last term in Eq. (13) is $1/Z^2$ small, and it can be neglected. In the following, we will adopt this approximation in order to arrive to a simple expression for the peaking factor.

Inserting the expressions for the drift and diamagnetic frequencies and using Eq. (1), it can be shown that the expression for the zero-flux impurity density gradient is

$$\frac{a}{L_{nz}^0}=2\frac{a}{R}\langle\mathcal{D}\rangle_\phi+s\kappa\frac{a}{r}\langle\theta\sin(\theta-\delta)\rangle_\phi, \tag{14}$$

where we introduced $\langle\ldots\rangle_\phi=\langle\ldots\mathcal{N}|\phi|^2/[(\omega_r-\omega_E)^2+\gamma^2]\rangle/\langle\mathcal{N}|\phi|^2/[(\omega_r-\omega_E)^2+\gamma^2]\rangle\simeq\langle\ldots\mathcal{N}|\phi|^2\rangle/\langle\mathcal{N}|\phi|^2\rangle$ and $\mathcal{N}(\theta)=\exp[\kappa\cos(\theta-\delta)]$. The second term in Eq. (14) stems from the $E_\theta\times B_\varphi$ drift, and it will be shown in Sec. IV that it is negative for inboard accumulation. Also the first term, containing $\langle\mathcal{D}\rangle_\phi$ (representing the curvature drift) is reduced for inboard accumulation, as it was pointed out in Refs. 6 and 7, but the reduction due to the second term is much larger, specially for moderate or large values of magnetic shear.

At this point, it is easy to demonstrate that including a non-zero $\partial\phi_E/\partial r$ would not change the impurity peaking significantly. By shifting the real part of the mode frequency in Eq. (2), as $\omega_r-(k_\theta/B)(\partial\phi_E/\partial r)\to\omega_r$, the gyrokinetic equation remains formally the same, as in the $\partial\phi_E/\partial r=0$ case, except that ω_r is different. In the large Z limit, considered above, ω_r appears only in the weighting factor of the $\langle\ldots\rangle_\phi$ average in Eq. (14), but not explicitly in the expression of the impurity peaking factor, thus it plays only a minor role; and accordingly, the effect of $\partial\phi_E/\partial r$ is small. This was verified numerically, including non-zero $\partial\phi_E/\partial r$ of different magnitudes in peaking factor calculations, yielding practically the same results as with $\partial\phi_E/\partial r=0$. However, it is important, that the radial electrostatic field corresponds to a toroidal rotation which, in turn, can contribute to the poloidal redistribution of heavy impurities due to centrifugal effects. Including finite Mach-number effects would require a significantly more complicated formalism that is out of the scope of the present work.

IV. PARAMETRIC DEPENDENCES OF THE PEAKING FACTOR

In the simulations, the following local profile and magnetic geometry parameters were used: $r/a=0.3$, $R/a=3$,

$k_\theta \rho_s = 0.3$, $q = 1.7$, $a/L_{ne} = 1.5, T_i/T_e = 0.85, a/L_{Te} = 2$, $a/L_{Ti} = 2.5$, $s = 0.22$, $\rho_s/a = 0.0035$, and $\hat{\nu}_{ei} = 0.0058\, c_s/a$ (collision frequency corresponding to $T_e = 7\,\mathrm{keV}, n_i = 3 \times 10^{19}\,\mathrm{m}^{-3}, \ln\Lambda = 17$, and $a = 1\,\mathrm{m}$). These parameters are similar to the ones used in Ref. 7, which will ease the comparison with those results. Nickel ($Z = 28$) impurity was assumed to be present in trace quantities, in the sense that $Zn_z/n_e \ll 1$ ($n_z/n_e = 2 \times 10^{-3}$ in the simulations). However, note that $Z^2 n_z/n_e \sim 1$, which implies that the strength of the poloidal asymmetry κ in Eq. (11) does not increase linearly with impurity charge Z. The temperatures and temperature gradients were assumed to be equal for the impurities and the main ions, $T_z/T_e = T_i/T_e$ and $a/L_{Tz} = a/L_{Ti}$. This is the baseline case in our study, and these parameters are used unless otherwise stated.

The perturbed electrostatic potential and eigenvalues were obtained by linear electrostatic gyrokinetic initial-value calculations with GYRO,[19] and it is assumed that they are unaffected by the presence of a weak poloidal variation of the electrostatic potential and the poloidally asymmetrically distributed *trace* impurity species. Linear initial-value studies only consider the most unstable mode and any subdominant modes are neglected. The main ion and electron densities are assumed to be approximately poloidally symmetric, which is important for the validity of the model. In the simulations, we use a model Grad-Shafranov magnetic equilibrium, where the $\mathcal{O}(\epsilon)$ corrections to the drift frequencies are retained. Flux-tube (periodic) boundary conditions were used, with a 128 point velocity space grid (8 energies, 8 pitch angles, and two signs of velocity), the number of radial grid points is 6, and the number of poloidal grid points along particle orbits is 20 for trapped particles. The location of the highest energy grid point is at $m_i v^2/(2T_i) = 6$. The ions were taken to be gyrokinetic and the electrons to be drift kinetic with the mass ratio $(m_i/m_e)^{1/2} = 60$.

A. Impurity species dependence

Figure 2 shows how the peaking factor varies for different impurity species with different charges. The model assumes moderate to high-Z impurities and accordingly $Ar^{+18}, Ni^{+28}, Mo^{+32}$, and W^{+40} were used, also because these impurities are present in existing experiments.[1–5,15] It is clear that the peaking factor is not sensitive to the charge number, neither in the symmetric nor in the asymmetric cases. This is in agreement with what has earlier been observed in both gyrokinetic and fluid simulations of transport dominated by ion temperature gradient (ITG) turbulence.[20] From Fig. 2, it is also evident that outboard impurity accumulation leads to an increase of the peaking factor with respect to the symmetric case, while in-out asymmetry leads to a substantial decrease. Furthermore, it is clear that a stronger asymmetry results in a larger shift in the peaking factor. Note that, from Eqs. (8) and (11), the strength of the poloidal asymmetry is expected to depend on the impurity charge and in the limit $Z^2 n_z/n_e \ll 1$ increase linearly with Z. However, this condition is not fulfilled in our baseline case (for instance, we have $Z^2 n_z/n_e \simeq 1.6$ for nickel). In this case, it can be shown that the asymmetry strength is almost the same

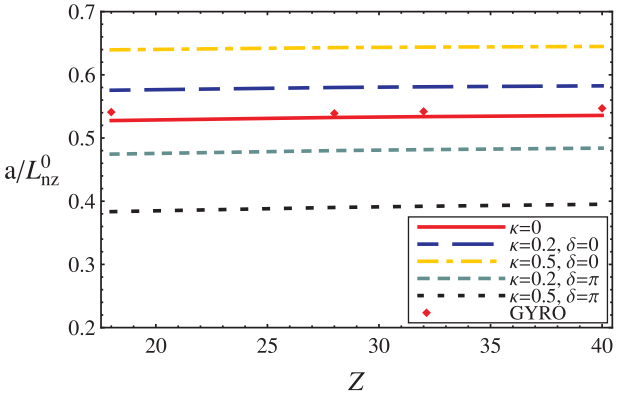

FIG. 2. Peaking factor as a function of impurity charge for different values of peaking angle δ and asymmetry strength κ. The red solid line represents the case of poloidally symmetric impurity distribution, and the diamonds represent GYRO values. $\kappa = 0.2$—out-in asymmetry (blue, wide dash-dotted line), $\kappa = 0.5$—out-in asymmetry (yellow, dash-dotted line), $\kappa = 0.2$—in-out asymmetry (green, dashed line), $\kappa = 0.5$—in-out asymmetry (black, dotted line). $Ar^{+18}, Ni^{+28}, Mo^{+32}$, and W^{+40} were used as ion species.

for Ar^{+18}, Ni^{+28}, Mo^{+32}, and W^{+40}, and our assumptions leading to the approximate expression for the peaking factor given in Eq. (14) are valid. As it is clear from Eq. (14), if we can treat the asymmetry strength κ as a parameter independent of Z, the impurity peaking factor will also be independent of Z to leading order because the $1/Z$ dependences of $\omega_{*z}, \hat{\omega}_{Dz}$ and ω_E cancel. We note that this reasoning would break down for $Z^2 n_z/n_e \ll 1$ when, for high Z, the GK equation and, accordingly, the impurity peaking factor would be dominated by the Z-independent ω_E.

B. Asymmetry dependence

From now on, we concentrate on the peaking factor for nickel ($Z = 28$), which has previously been studied in Ref. 7 and was also one of the main impurities studied in Ref. 1. In Fig. 3, it is shown how the peaking factor for nickel varies with asymmetry strength κ for both out-in and in-out asymmetries. From the previous results of Refs. 6 and 7 (valid in the limit of negligible ω_E), we expect that an inboard asymmetry leads to a reduction of the peaking factor, and this is indeed the case as Fig. 3 shows. It is interesting to note that for the weak asymmetry used here the presence of ω_E is crucial to obtain a sizable reduction. For comparison, in Fig. 3, the $\omega_E = 0$ case is shown with dotted line, and it is clear that if the $E_\theta \times B_\varphi$ drift is neglected, the peaking factor is almost unaffected by the poloidal asymmetry up to $\kappa \simeq 1$. This is in agreement with the results of Ref. 7, where much larger asymmetry strengths were used to obtain a reduction for the peaking factor.

Figure 3 suggests that an in-out asymmetry leads to a decrease in peaking factor while an out-in asymmetry will increase it. It is also clear that the change in the peaking factor, irrespective of if it is an increase or decrease, is greater the higher the asymmetry strength.

C. Shear dependence

As we have seen in Sec. IV B, a sign-change in the peaking factor (for low shear, as we assumed in our baseline

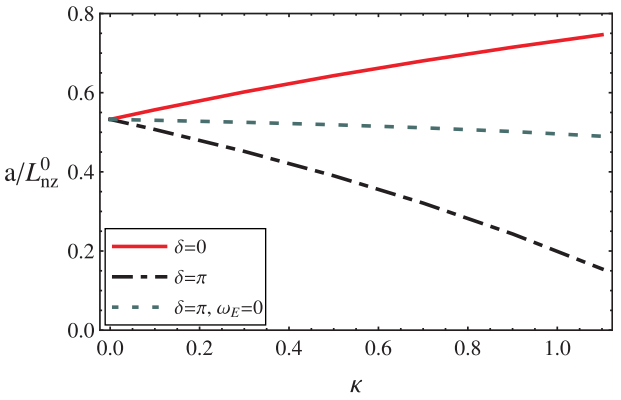

FIG. 3. Peaking factor for nickel as a function of asymmetry strength κ with out-in asymmetry (red, solid line) and in-out asymmetry (black, dash-dotted line). The gray dotted curve represents in-out asymmetry with ω_E neglected, comparing this curve to the corresponding curve with ω_E included (black, dash-dotted line) illustrates the impact which the $E_\theta \times B_\varphi$ drift has on the peaking factor.

parameters) would require a much larger level of asymmetry than what could be explained by ICRH driven impurity asymmetry, where $\kappa \lesssim 0.5$ even for high Z and large temperature anisotropies. However, the asymmetry in the moderate shear region is one of the most important factors leading to a large change in the peaking factor, which (as we will see later) is quite insensitive to other plasma parameters.

Figure 4(a) shows that the peaking factor is very sensitive to the shear. The main reason for the shear-dependence is the $E_\theta \times B_\varphi$ drift term. This fact is also evident from the approximate analytical expression for the peaking factor Eq. (14), where the shear-dependence is explicit in the term that stems from ω_E. For $\kappa = 0.5$ and $s = 1$, even a sign-change occurs. The behavior is very different from the symmetric case, where the peaking factor is expected to increase with shear. The reduction of the peaking factor occurs only in the case of inboard accumulation (for positive shear). In the case of out-in asymmetry, instead a large increase in the peaking factor is expected. In Fig. 4(a), we also plot the approximate peaking factors corresponding to Eq. (14) with dotted curves, demonstrating that this simple formula reproduces the shear dependence remarkably well.

Figure 4(b) shows the shear-dependence of the eigenvalues. The real frequency is significantly reduced for low or negative shear. Also, the imaginary part of the perturbed potential is quite sensitive to the shear. However, the shear-dependence of the imaginary part of the perturbed potential and the real part of the eigenfrequency are not enough to influence the peaking factor significantly, since the sensitivity to the shear is not observed without the ω_E term.

The curves for the peaking factor for various asymmetries cross very close to $s = 0$ (see Fig. 4(a)), which can be explained by the fact that for $s = 0$ the $E_\theta \times B_\varphi$ drift-term $\omega_E = 0$ and the main reason for the change in the peaking factor disappears. Note, that in the case of negative shear, the behavior is opposite to that of positive shear. Then, inboard asymmetries lead to larger peaking factors. This is due to the fact that ω_E changes sign for negative shear.

Previous work investigating the effect of poloidal asymmetries on impurity transport[6,7] did not include the $E_\theta \times B_\varphi$ drift term. In the limit of $\omega_E = 0$ and no collisions, our model reproduces the results of Ref. 7. Our present results, however, suggest that the $E_\theta \times B_\varphi$ drift frequency is in fact the main reason why a poloidal asymmetry can result in a reduction of the impurity peaking factor. To understand why these results are seemingly different from the results of Ref. 7, it should be noted that the poloidal asymmetry is introduced differently in the two models, as mentioned at the end of Sec. III. In Ref. 7, the significant reduction of the peaking factor was observed for much larger asymmetry strengths $n \gtrsim 2.5$. The maximum asymmetry strength used here $\kappa = 0.5$ corresponds to the sum of two terms: $n = 0$ with weight $f_0 = 1$ and $n = 1$ with $f_1 = 2$. Then the total peaking factor can be estimated to be

$$\frac{a}{L^0_{nz}} \simeq \frac{f_0}{f_0 + f_1}\frac{a}{L_{nz0}} + \frac{f_1}{f_0 + f_1}\frac{a}{L_{nz1}},$$

where a/L_{nz0} is the peaking factor corresponding to the poloidally symmetric part ($n = 0$, with weight f_0), and a/L_{nz1}

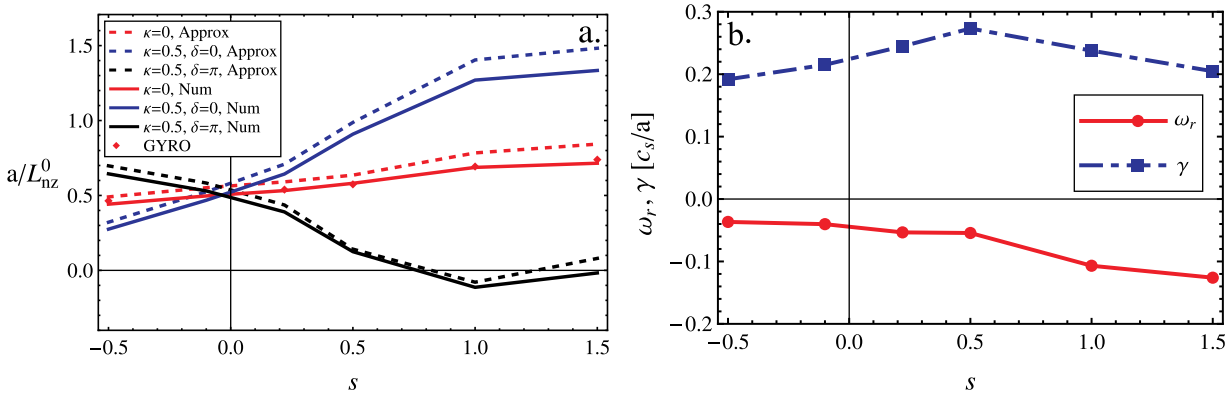

FIG. 4. (a) Peaking factor for nickel as a function of shear s for different values of peaking angle δ and asymmetry strength $\kappa = 0.5$. Symmetric impurity density (red line), out-in asymmetry (blue line), and in-out asymmetry (black line). Diamonds correspond to GYRO results. The figure also shows a comparison between the numerical solution in Eq. (6) (Num.) represented by solid lines and the analytical approximation in Eq. (14) (Approx.) represented by dotted lines. (b) Real and imaginary parts of $\omega = \omega_r + i\gamma$ as functions of shear s. Red line (with circle markers) represents the real part, and blue dash-dotted line (square markers) represents the imaginary part of the eigenvalues. Frequencies are normalized to c_s/a.

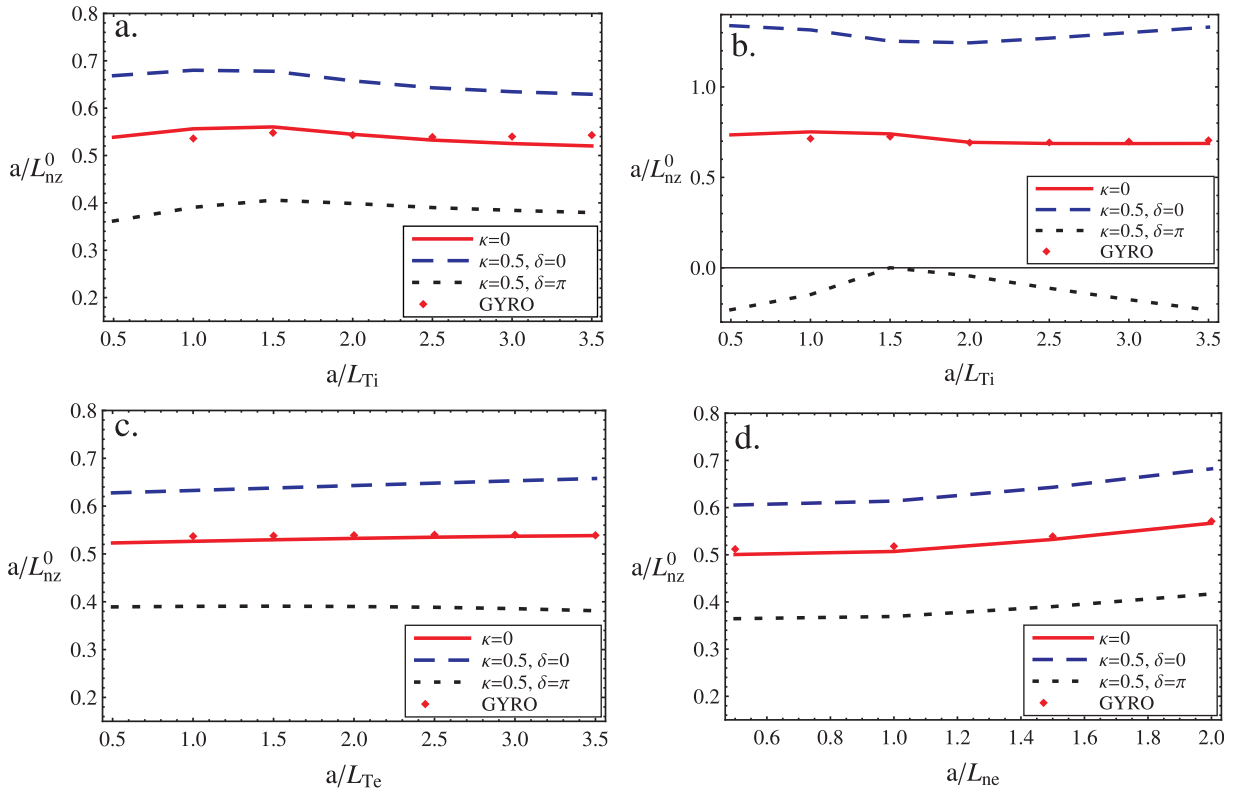

FIG. 5. Peaking factor for nickel as a function of ion temperature gradient a/L_{Ti} with $s = 0.22$ (a) (the baseline case) and $s = 1$ (b), electron temperature gradient a/L_{Te} (c) and electron density gradient a/L_{ne} (d) for different values of peaking angle δ and asymmetry strength $\kappa = 0.5$. Symmetric impurity density (red, solid line), out-in asymmetry (blue, dashed line), and in-out asymmetry (black, dotted line). Diamonds correspond to GYRO results.

is the peaking factor corresponding to the poloidally asymmetric part ($n = 1$, with weight f_1). The peaking factor in this case would then be $a/L^0_{nz} \simeq (1/3)(a/L_{nz0}) + (2/3)(a/L_{nz1})$. The term with $n = 1$ gives a slight reduction of the peaking factor, but the total peaking factor is almost unaffected.

From Eq. (14), we can also see that the temperature and density gradients of the electrons and main ions neither affect the impurity peaking directly nor through the mode frequencies and growth rates to leading order in $1/Z$. The effect of these gradients appear mainly through the form of the ballooning eigenfunction (and through higher order terms in $1/Z$), and it is rather weak as it is illustrated in Fig. 5.

D. Effect of collisions

In the baseline case of our study, the turbulence is ITG mode dominated (the real part of the mode frequency $\omega_r = -0.053 c_s/a$ is negative). For ITG mode dominated plasmas, the collisionality is expected to have a small impact on the transport.[21] This is shown in Fig. 6, where both mode

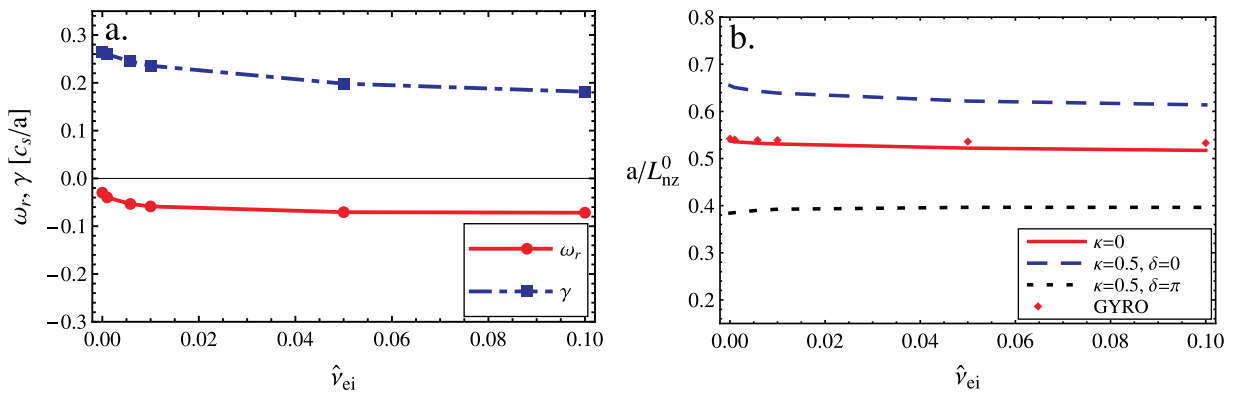

FIG. 6. (a) Real and imaginary parts of $\omega = \omega_r + i\gamma$ as functions of electron-ion collision frequency $\hat{\nu}_{ei}$. Red line (with circle markers) represents the real part, and blue dash-dotted line (square markers) represents the imaginary part of the eigenvalues. Frequencies are normalized to c_s/a, and the baseline case is $\hat{\nu}_{ei} = 0.0058\, c_s/a$. (b) Peaking factor for nickel as a function of electron-ion collision frequency $\hat{\nu}_{ei}$ for different values of peaking angle δ and asymmetry strength $\kappa = 0.5$. Symmetric impurity density (red, solid line), out-in asymmetry (blue, dashed line), and in-out asymmetry (black, dotted line). Diamonds correspond to GYRO results.

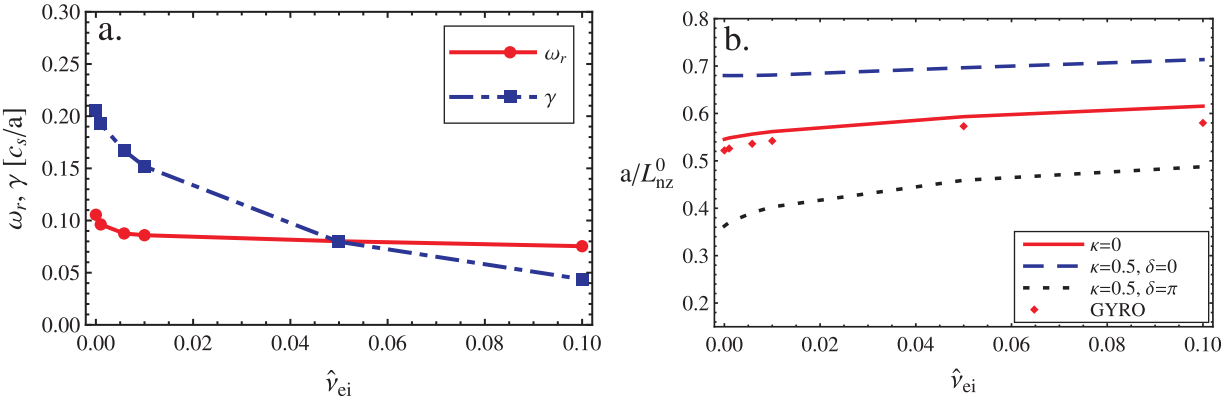

FIG. 7. Collisionality dependence for a TEM dominated plasma obtained by changing the ion and impurity temperature gradients to $a/L_{Ti} = a/L_{Tz} = 1.0$ in the baseline case. (a) Real and imaginary parts of $\omega = \omega_r + i\gamma$ as functions of electron-ion collision frequency $\hat{\nu}_{ei}$. Red line (with circle markers) represents the real part; blue dash-dotted line (square markers) represents the imaginary part of the eigenvalues. Frequencies are normalized to c_s/a. (b) Peaking factor for nickel as a function of electron-ion collision frequency $\hat{\nu}_{ei}$ for different values of peaking angle δ and asymmetry strength $\kappa = 0.5$. Symmetric impurity density (red, solid line), out-in asymmetry (blue, dashed line), and in-out asymmetry (black, dotted line). Diamonds correspond to GYRO results.

frequency and impurity peaking factor are almost unaffected by a change in electron-ion collision frequency. The poloidally asymmetric cases are also only weakly affected by a change in collisionality; hence, neglecting the collision operator in the GK equation (Eq. (4)) would be an approximation which would not induce a significant error in this particular study.

To see why the impurity peaking is rather insensitive to collisions, we consider two limits of Eq. (7). In the collisionless limit, it reduces to $A = (35\bar{F}_0 + 10\bar{F}_2)/(35\bar{F}_0^2 + 10\bar{F}_0\bar{F}_2 - 7\bar{F}_2^2)$. After substituting, the definitions of $\bar{F}_0$ and $\bar{F}_2$ into this expression we can expand in $\bar{\omega}_{D0}$ to first order (that is relevant for high Z) to find the approximate expression

$$A \approx \frac{i}{\bar{\omega} - \bar{\omega}_E}\left[1 + \frac{2\bar{\omega}_{D0}x^2}{3(\bar{\omega} - \bar{\omega}_E)}\right]. \tag{15}$$

Interestingly, in the opposite limit ($\bar{\nu}_D \to \infty$) when $A \approx 1/\bar{F}_0$, a similar expansion in $\bar{\omega}_{D0}$ leads to the same result as Eq. (15). This means that the collisions can only affect the impurity peaking through their effect on the mode frequencies and mode structure, or through terms that are higher order in $\bar{\omega}_{D0} \propto 1/Z$.

By changing the ion and impurity temperature gradients to $a/L_{Ti} = a/L_{Tz} = 1.0$ in the baseline case, a TEM (trapped electron mode) dominated plasma is obtained. Figure 7 shows how the eigenvalues and the impurity peaking factor for this plasma depend on collision frequency. As expected in a TEM dominated plasma, an increase in collisionality leads to a suppression of instabilities seen from the reduction of the growth rate γ. Compared to the ITG mode dominated plasma, the peaking factor is more affected by collisionality in the TEM case even though the dependence is still rather weak (compare Fig. 7(b) with Fig. 6(b)). The reason for this is that the mode frequency, in particular the growth rate, is more influenced by a change in collision frequency for the TEM case than for the ITG case. Consequently, the peaking factor is rather affected indirectly by a change in collision frequency through the change in mode frequency, than directly by the change in collision frequency itself.

V. DISCUSSION AND CONCLUSIONS

We have studied the effect of the $E_\theta \times B_\varphi$-drift and collisions on high-Z trace impurity transport driven by electrostatic turbulence in the presence of poloidal asymmetries. For simplicity, we have used a large aspect ratio, circular cross section equilibrium, and neglected impurity parallel motion, electrostatic trapping, and FLR-effects (which are good approximations for heavy impurities). We assumed that impurity self-collisions dominate and modeled the collisions with a Lorentz operator.

The main result of the paper is that—as soon as there is a poloidally asymmetric equilibrium electrostatic potential ϕ_E in tokamaks so that $Ze\phi_E/T_z$ is order unity—the asymmetry and shear are the two most important parameters that govern the peaking of moderate and high-Z impurities. The shear dependence of the impurity peaking is mainly due to the $E_\theta \times B_\varphi$ drift term in the gyrokinetic equation. For moderate shear, the peaking factor is substantially reduced and changes sign for inboard accumulation. The other plasma parameters, such as collisionality, ion and electron temperature gradients and electron density gradient do not influence the peaking factor significantly. Experimentally the presented results could be most easily checked by magnetic shear scans in discharges with low field side ICRH heating.

Although in the present paper only the ICRH generated poloidal potential variation was discussed in more detail, the formalism presented is valid for any situation when there is a poloidal electric field causing a poloidally asymmetric impurity distribution. From the reasoning of Sec. III, it is expected that ECRH causes a temperature anisotropy in the electron distribution, increasing the trapped electron population close to the resonant layer. If the resonant layer is in the high field side, it sets up a potential that leads to an inboard impurity accumulation and decreasing impurity peaking. For low field side ECRH heating, the opposite effect is expected. Experimental measurement of impurity asymmetries and peaking, depending on the location of the resonant layer in both ion and electron cyclotron heated plasmas would be an important step towards the understanding of impurity transport in RF heated plasmas.

This paper considers the situation when the poloidal asymmetry of impurities is purely caused by the poloidal variation of the electrostatic potential, but centrifugal effects can also be important especially in strongly rotating plasmas with neutral beam injection (NBI). Temperature anisotropy for the main ions is also generated in NBI plasmas which, together with the centrifugal effects on the main ions, also contribute to the poloidally varying potential. The value of $T_{\perp i}/T_{\|i}$ depends on the injection geometry, being higher than unity for perpendicular and lower for tangential injection. In this case, a more sophisticated model is necessary to calculate the poloidal variation of the potential and the impurity density.

ACKNOWLEDGMENTS

The authors gratefully acknowledge the discussions with P. Helander, F. Parra, P. Catto, M. Reinke, and M. Landreman and would like to thank J. Candy for providing the GYRO code. This work was funded by the European Communities under Association Contract between EURATOM and *Vetenskapsrådet*. The views and opinions expressed herein do not necessarily reflect those of the European Commission.

APPENDIX A: DERIVATION OF ω_E

We define ω_E through $\mathbf{v}_E \cdot \nabla g_z = -i\omega_E g_z$, where $\mathbf{v}_E$ is the $\mathbf{E}\times\mathbf{B}$ drift velocity due to the equilibrium electrostatic field. To obtain the expression (3) for ω_E, we first note that for an axisymmetric field ϕ_E and a perturbed scalar field g_z (satisfying $\nabla_\| g_z \ll \nabla_\perp g_z$), for a low-beta, circular plasma

$$\mathbf{B}\times\nabla\phi_E\cdot\nabla g_z = -\frac{\partial g_z}{\partial\alpha}\frac{\partial\phi_E}{\partial\psi}B^2 - \frac{\partial g_z}{\partial\alpha}\frac{\partial\phi_E}{\partial z}(\nabla\alpha\times\nabla z)\cdot\mathbf{B} - \frac{\partial g_z}{\partial\psi}\frac{\partial\phi_E}{\partial z}(\nabla\psi\times\nabla z)\cdot\mathbf{B}. \tag{A1}$$

This expression can be obtained from Eq. (4) of Ref. 22. Here, z measures the distance along the field line, ψ is the poloidal flux, $\alpha \approx \zeta - q\vartheta$ is the binormal coordinate with the toroidal and poloidal angles ζ and ϑ, and the magnetic field can be written as $\mathbf{B} = \nabla\alpha\times\nabla\psi$. In the simple geometry we consider, we have $(\nabla\alpha\times\nabla z)\cdot\mathbf{B} \approx -Bq_0 s\vartheta/r_0^2$ and $(\nabla\psi\times\nabla z)\cdot\mathbf{B} \approx B_0^2/q$. By introducing a rescaled binormal coordinate $y = -\alpha r/q$, and using the relation between the minor radius and the poloidal flux $\psi - \psi_0 \approx xB_0 r_0/q_0$ with $x = r - r_0$, furthermore using the relation between the radial and binormal wave numbers $k_x = k_y s\vartheta_0$ in terms of the ballooning angle ϑ_0, Eq. (A1) can be rewritten as

$$\mathbf{B}\times\nabla\phi_E\cdot\nabla g_z = ik_y B\left[\frac{\partial\phi_E}{\partial r} - \frac{1}{r}\frac{\partial\phi_E}{\partial\vartheta}s(\vartheta-\vartheta_0)\right]g_z. \tag{A2}$$

With the choice $\vartheta_0 = 0$ that is usually true for the most unstable mode, Eq. (3) follows immediately.

APPENDIX B: VARIATIONAL SOLUTION OF THE GK EQUATION INCLUDING COLLISIONS MODELED BY A LORENTZ OPERATOR

The eigenfunctions of the differential operator

$$\mathcal{L} = \frac{\partial}{\partial\xi}\left[(1-\xi^2)\frac{\partial}{\partial\xi}\right]$$

are the Legendre polynomials $\mathcal{L}P_n(\xi) = -n(n+1)P_n(\xi)$, which are orthogonal on $[-1,1]$: $\int_{-1}^{1} d\xi P_n(\xi)P_m(\xi) = 2\delta_{mn}/(2n+1)$. We aim to find an approximate solution for g_z in the form of a truncated Legendre polynomial series $g_z(x,\xi) = \sum_n g_n(x)P_n(\xi)$, where only the $P_0(\xi) = 1$ and $P_2(\xi) = (3\xi^2-1)/2$ terms are kept (P_1 and other odd polynomials disappear upon velocity space integration). Consequently, $g_z(x,\xi) \approx g_0(x)P_0(\xi) + g_2(x)P_2(\xi)$. Using this approximation, Eq. (4) can be rewritten as

$$\Big(P_0(\xi)F_0(x) + P_2(\xi)F_2(x)\Big)\Big(P_0(\xi)g_0(x) + P_2(\xi)g_2(x)\Big) + 3\nu_D(x)P_2(\xi)g_2(x) = P_0(\xi)f_S(x), \tag{B1}$$

where $F_0(x) = -i(\omega - 2\omega_{Dx}/3 - \omega_E)$, $F_2(x) = i\omega_{Dx}/3$, and $f_S(x) = -iZef_{z0}(\omega - \omega_{*z}^T)\phi/T_z$. This equation is solved approximately by adopting a variational approach, and minimizing the functional

$$\Lambda = \int_{-1}^{1} d\xi (P_0 g_0 + P_2 g_2)[(P_0F_0 + P_2F_2) \times (P_0 g_0 + P_2 g_2) + 3\nu_D P_2 g_2 - 2P_0 f_S]. \tag{B2}$$

Utilizing the orthogonality relation for Legendre polynomials and that $\int_{-1}^{1} d\xi P_2^3(\xi) = 4/35$, integration yields

$$\Lambda = 2(F_0 g_0^2 - 2f_S g_0) + \frac{4}{35}F_2 g_2^2 + \frac{2}{5}(2F_2 g_0 g_2 + F_0 g_2^2 + 3g_2^2\nu_D). \tag{B3}$$

The coefficients g_0 and g_2 that minimize the functional must satisfy

$$\frac{\partial\Lambda}{\partial g_0} = 4\left[F_0 g_0 - f_S + \frac{1}{5}F_2 g_2\right] = 0,$$

$$\frac{\partial\Lambda}{\partial g_2} = \frac{8}{35}F_2 g_2 + \frac{4}{5}(F_2 g_0 + F_0 g_2 + 3g_2\nu_D) = 0.$$

The solution of this linear system is

$$g_0 = 5f_S(7F_0 + 2F_2 + 21\nu_D)/A_2,\quad g_2 = -35F_2 f_S/A_2,\quad A_2 = 35F_0^2 + 10F_0F_2 - 7F_2^2 + 105F_0\nu_D, \tag{B4}$$

and the non-adiabatic part of the perturbed impurity distribution function becomes

$$g(x,\xi) = g_0(x)\,P_0(\xi) + g_2(x)\,P_2(\xi) = A_1(x,\xi) f_S(x)/A_2(x), \tag{B5}$$

where

$$A_1(x,\xi) = 5\Big(7F_0(x) + 2F_2(x) + 21\nu_D(x)\Big)P_0(\xi) - 35F_2(x)\,P_2(\xi).$$

[1]M. Valisa, L. Carraro, I. Predebon, M. E. Puiatti, C. Angioni, I. Coffey, C. Giroud, L. Lauro Taroni, B. Alper, M. Baruzzo, P. Belo daSilva, P. Buratti, L. Garzotti, D. Van Eester, E. Lerche, P. Mantica, V. Naulin, T. Tala, M. Tsalas, and JET-EFDA Contributors, Nucl. Fusion **51**, 033002 (2011).
[2]R. Dux, R. Neu, A. G. Peeters, G. Pereverzev, A. Muck, F. Ryter, J. Stober, and ASDEX Upgrade Team, Plasma Phys. Controlled Fusion **45**, 1815 (2003).
[3]M. E. Puiatti, M. Valisa, M. Mattioli, T. Bolzonella, A. Bortolon, I. Coffey, R. Dux, M. von Hellermann, P. Monier-Garbet, M. F. F. Nave, J. Ongena, and Contributors to the EFDA-JET Workprogramme, Plasma Phys. Controlled Fusion **45**, 2011 (2003).
[4]M. E. Puiatti, M. Valisa, C. Angioni, L. Garzotti, P. Mantica, M. Mattioli, L. Carraro, I. Coffey, C. Sozzi, and JET-EFDA Contributors, Phys. Plasmas **13**, 042501 (2006).
[5]R. Neu, R. Dux, A. Kallenbach, T. Putterich, M. Balden, J. C. Fuchs, A. Herrmann, C. F. Maggi, M. O'Mullane, R. Pugno, I. Radivojevic, V. Rohde, A. C. C. Sips, W. Suttrop, A. Whiteford, and ASDEX Upgrade Team, Nucl. Fusion **45**, 209 (2005).
[6]T. Fülöp and S. Moradi, Phys. Plasmas **18**, 030703 (2011).
[7]S. Moradi, T. Fülöp, A. Mollén, and I. Pusztai, Plasma Phys. Controlled Fusion **53**, 115008 (2011).
[8]J. L. Terry, E. S. Marmar, K. I. Chen, and H. W. Moos, Phys. Rev. Lett. **39**, 1615 (1977).
[9]M. Romanelli and M. Ottaviani, Plasma Phys. Controlled Fusion **40**, 1767 (1998).
[10]T. Fülöp and P. Helander, Phys. Plasmas **6**, 3066 (1999).
[11]T. Fülöp and P. Helander, Phys. Plasmas **8**, 3305 (2001).
[12]M. Landreman, T. Fülöp, and D. Guszejnov, Phys. Plasmas **18**, 092507 (2011).
[13]M. Reinke, Ph.D. dissertation, Massachusetts Institute of Technology, 2011.
[14]L. C. Ingesson, H. Chen, P. Helander, and M. J. Mantsinen, Plasma Phys. Controlled Fusion **42**, 161 (2000).
[15]M. L. Reinke, I. H. Hutchinson, J. E. Rice, N. T. Howard, A. Bader, S. Wukitch, Y. Lin, D. Pace, A. Hubbard, J. W. Hughes, and Y. Podpaly, Plasma Phys. Controlled Fusion **54**, 045004 (2012).
[16]R. D. Hazeltine and J. D. Meiss, *Plasma Confinement* (Dover, 2003).
[17]J. P. Graves, W. A. Cooper, S. Coda, L.-G. Eriksson, T. Johnson, and JET-EFDA Contributors, AIP Conf. Proc. **871**, 350 (2006).
[18]Ye. O. Kazakov *et al.*, "Poloidal asymmetries due to ion cyclotron resonance heating," Plasma Phys. Controlled Fusion (submitted).
[19]J. Candy and R. E. Waltz, J. Comput. Phys. **186**, 545 (2003).
[20]H. Nordman, A. Skyman, P. Strand, C. Giroud, F. Jenko, F. Merz, V. Naulin, T. Tala, and JET-EFDA Contributors, Plasma Phys. Controlled Fusion **53**, 105005 (2011).
[21]I. Pusztai, T. Fülöp, J. Candy, and J. R. Hastie, Phys. Plasmas **16**, 072305 (2009).
[22]M. A. Beer, S. C. Cowley, and G. W. Hammett, Phys. Plasmas **2**, 2687 (1995).